Copyright Warning & Restrictions

The copyright law of the United States (Title 17, United States Code) governs the making of photocopies or other reproductions of copyrighted material.

Under certain conditions specified in the law, libraries and archives are authorized to furnish a photocopy or other reproduction. One of these specified conditions is that the photocopy or reproduction is not to be "used for any purpose other than private study, scholarship, or research." If a, user makes a request for, or later uses, a photocopy or reproduction for purposes in excess of "fair use" that user may be liable for copyright infringement,

This institution reserves the right to refuse to accept a copying order if, in its judgment, fulfillment of the order would involve violation of copyright law.

Please Note: The author retains the copyright while the New Jersey Institute of Technology reserves the right to distribute this thesis or dissertation

Printing note: If you do not wish to print this page, then select "Pages from: first page # to: last page #" on the print dialog screen

Abstract

Title of Thesis : Properties of sputtered a-Ge and a-Ge:H thin films

Hanjin Cho, Master of Science in Electrical Engineering , 1987

Thesis directed by : Dr. Kenneth S. Sohn.

The effect of the amorphous and glassy structure of amorphous germanium films on their electrical characteristics was investigated experimentally. The films were deposited onto silicon substrates using a modified MRC 8800 triode sputtering system. The Poole-Frenkel and Schottky mechanisms are discussed in detail and the shortcomings of the accepted picture of the former in amorphous materials are dealt with. It was concluded on the basis available evidence that the current flow in amorphous germanium favors the Poole-Frenkel mechanism at high fields.

Amorphous hydrogenated germanium films which were deposited by bias sputtering were characterized by measuring the infrared absorption. The films have absorption peaks,as expected, at 1950 cm^{-1} and at 570 cm^{-1} due to GeH_2 bonding and at 1880 cm^{-1} due to GeH bonding.

A method was described for determining the optical constants of a thin film deposited on a nonabsorbing window using a single set of transmittances over an absorption

band. The method depends on the fact that the phase shift of the transmitted radiation can be determined from the transmittance by a Kramers-Kronig transform. The transmittance data of a-Ge:H and sputtered silicon nitride films were used to calculate their optical constants by this method. In a-Ge:H films, the value of the calculated refractive index in the k=0 region was not reasonable. However, for Si_3N_4 films, the calculated absorption coefficient was consistent with the experimental results.

PROPERTIES OF SPUTTERED

a-Ge and a-Ge:H THIN FILMS

by

Hanjin Cho

Thesis submitted to the Faculty of the Graduate School of
the New Jersey Institute of Technology in partial fulfilment of
the requirement for the degree of
Master of Science in Electrical Engineering
1987

APPROVAL SHEET

Title of Thesis: Properties of Sputtered a-Ge and a-Ge:H thin films

Name of Candidate: Hanjin Cho

Master of Science in Electrical Engineering

1987

Thesis and Abstract Approved:

Dr. Kenneth S. Sohn — Date
Professor
Department of Electrical Engineering

Dr. Roy H. Cornely — Date
Professor
Department of Electrical Engineering

Dr. Warren H. Ball — Date
Associate chairman
Department of Electrical Engineering

VITA

Name: Hanjin Cho

Degree and date to be conferred: Master of Science in EE,1987

Secondary education: Kyung-Dong High school (Korea), 1978

Collegiate institutions attended	Dates	Degree	Date of degree
Hanyang University (Korea)		B.S.	Feb. 1982
New Jersey Inst. of Tech.		M.S.	May 1987

Major: Electrical Engineering

Dedicated

to

my parents and wife

ACKNOWLEDGEMENTS

I am indebted to many people for their guidance and advice about this research. I would like to offer my inadequate acknowledgement of appreciation to Dr. Kenneth S. Sohn and Dr. Roy H. Cornely whom without this research would have not been possible. I would like to thank my fellow graduate and undergraduate students,especially Mr. Rajenda, who assisted me throughout my work. Finally, I would like to express my gratitude to my family who believed in me and gave me encouragement and support to achieve my greatest goal of all.

TABLE OF CONTENTS

LIST OF TABLES

LIST OF FIGURES

I. INTRODUCTION

Transport in amorphous Ge thin films is generally supposed to proceed by two qualitatively different mechanisms: the first, which is dominant at relatively high temperatures, involves the motion of conduction-band electrons and valence-band holes among the states intrinsic to the completely coordinated, but disordered, network; the second, which is dominant at low temperatures, involves the transport (by tunneling of hopping or both) of carriers between extrinsic states with energies in the psuedogap. Understanding of the origin and properties of these extrinsic states is essential to the establishment of an adequate description of the semiconductor. Structural measurements (1) have shown that sputtered a-Ge films contain a distribution of voids of the order of 5-10 A diameter. Optical, transport, and electron-spin-resonance measurement (2,3) have been plausibly and self-consistently interpreted on a model which identifies the majority of pseudogap electrons with those on these internal void surfaces. Controlled addition of hydrogen to the sputtering gas (4,5) produces profound systematic changes in properties, which are easily understood on the supposition that the hydrogen forms a strong bond with Ge atoms on void surfaces, and thereby eliminates states from the pseudogap.

Hydrogen, with its single electron and its small covalent radius, can be used to compensate individual dangling bonds on the void surfaces of amorphous Ge, and the variations of the electronic properties with hydrogen coverage can be determined. Thus the density of electronic states of fully bonded but hydrogenated amorphous Ge, which near the gap will resemble that of fully coordinated material, can in principle be established (5). The advantages of this new technique over the traditional approaches to minimize the number of effects of dangling bonds, i.e., annealing using an elevated substrate temperature during deposition, are numerous. The traditional methods in addition to modifying the void structure also modify the network itself and both effects contribute inseparably to the changes of the properties. Furthermore, it is difficult to measure directly whether all dangling bonds have been removed after a certain thermal treatment. In contrast, hydrogenation does not suffer from these deficiencies. Hydrogen may be added till saturation of the void surfaces occurs and the properties can be observed at this juncture. Moreover, a study of the effects of annealing n the properties of saturated material demonstrates the effects of network reorganization.

Lewis (4) has made an extensive study of the conductivity and themoelectric power as a function of temperature for samples of different hydrogen content prepared by rf sputtering. He suggested that high temperature transport

occurs by small-polaron hopping. Moustakas and Paul (6) reported steady-state and transient-photoconductivity studies on a series of amorphous Ge thin films with different hydrogen concentrations. They proposed a model that the photocarriers form small polarons out of the band states and that these polarons degrade in energy by phonon emission, all the while transporting current by moving in the applied field, until their contribution to conductance is no longer significant. At the lower temperatures, the polaron formed out of intrinsic states gradually changes into a polaron formed out of defect pseudogap states, without scattering abruptly into states of appreciably lower energy. Thus, the density of pseudogap states, which may be affected by hydrogenation, has only a weak effect on the time for the polaron to degrade. At the higher temperatures, there exists the possibility that the polaron may gain energy from the lattice, depending on the ratio of kT to its binding energy.

Rudder et al. (7) reported that amorphous Ge:H films by magnetron sputtering have $\mu\tau$ products at least an order of magnitude higher than the best previously reported which was grown by diode sputtering of glow discharge methods.

The principles and background information concerning rf sputtering as a process for deposition of a-Ge and a-Ge:H films are given in chapter IV. The properties of amorphous thin films are sensitive to the details of the preparation

conditions. Our goal has been to carefully control the preparation conditions in order to better understand the effect of each deposition parameter on the properties of films. The current transport mechanisms through amorphous germanium films deposited by diode sputtering at different argon partial pressure are examined in chapter II. In chapter III, hydrogenated germanium films deposited by bias sputtering are characterized by infrared spectra using Perkin-Elmer model 457 spectrophotometer. Particular attention has been given to find the optimum ratio of partial pressure of hydrogen to argon and optimum rf-induced substrate bias voltage. In chapter IV, the digital computer method to determine optical constants n,k of thin films is discussed.

II. Electrical Properties of Amorphous Germanium.

2.1. Theory and background

In this chapter current transport mechanisms through amorphous Ge films at low and high electric fields (> $2x10^6$ V/cm) are examined.

Theoritical studies of amorphous semiconductors indicate (1) that even though long-range order is not preserved , as long as molecular bonds are not significantly distrubed, an energy bond model is still applicable. For a more detailed discussion, a review by Mott (2) should be consulted. The Poole-Frenkel and Schottky mechanisms are discussed in detail in Section A. Johnscher (3) concluded that it is not yet possible to rule out definitely either the former or the latter of these effects in any particular case and that electronic hopping in dielectric films is the dominant conduction mechanism at low fields and at moderate high fields. Walley and Jonscher (4) reported that the value of field-lowering coefficients from their sputtered a-Ge films was about twice the expected theoretical value for the presence of Poole-Frenkel effect and four times the expected theoretical value for Schottky emission. Feldman (10), however, observed power-law dependence of current upon voltage, i.e, current is proportional to the exponents

the range 6-8 of voltage.

Of these two interpretations, the data presented in this paper favor the Poole-Frenkel mechanism.

A. The Poole-Frenkel Effect and its interpretation

The Poole-Frenkel effect is being invoked very frequently in the interpretation of the electric current in dielectric films at resonably high electric fields.

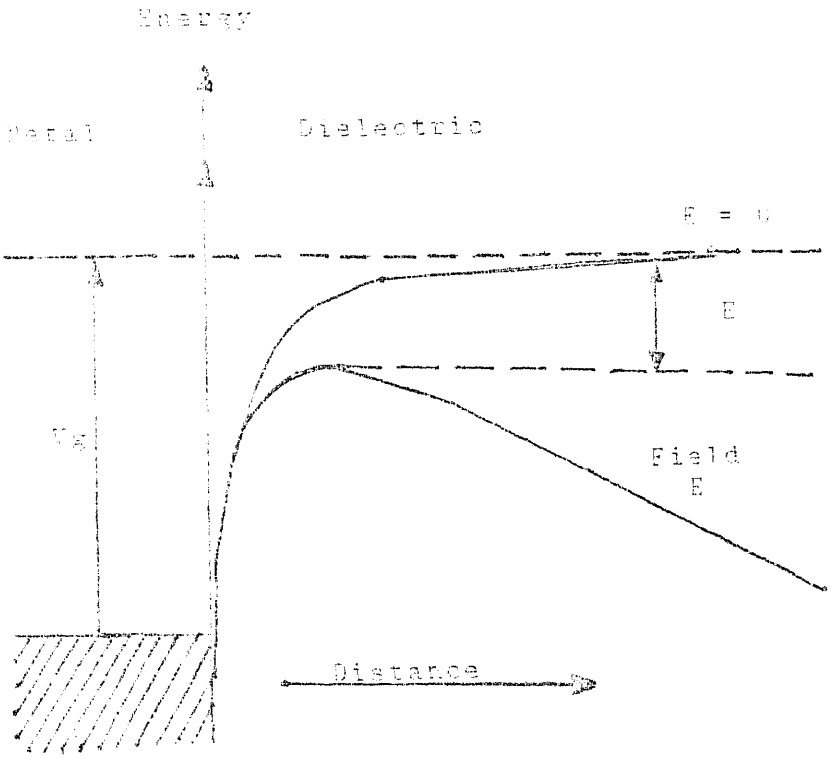

Fig. 2-1. The Schottky effect with a planar cathode.

The physical basis of this effect is analogous to the Schottky effect for a plane electrode - a lowering of the potential barrier Vg surrounding a localized charge under the influence of an external electric field. The Schottky effect is thermionic emission over a field-lowered barrier (Fig. 2-1), and the expression is usually written in the form

$$I = Io \exp \left[\frac{e\ (\beta\ E^{\frac{1}{2}} - Vg)}{k\ T} \right] \qquad (1)$$

where the Schottky field-lowering coefficients is given by

$$\beta s = \left(\frac{e}{4\ \pi\ \epsilon_o\ \epsilon} \right)^{\frac{1}{2}}$$

where ϵ_o is the permittivity of free space and ϵ the relative dielectric permittivity (dielectric constant). In the case of a point defect surrounded by a Coulombic potential, the Poole-Frenkel effect is obtained (5), and the field-lowering of the barrier height is now given by $\beta_{PF}E^{\frac{1}{2}}$, where the Poole-Frenkel coefficient $\beta_{PF} = 2\beta_S$, on account of different geometry.

It is well established experimental fact (6) that at fields in excess of some 10^4 V/cm many dielectric films exhibit current-voltage characteristics of the form

$$I = C\ E\ \exp \left(\frac{e\ \beta\ E^{\frac{1}{2}}}{k\ T} \right) \qquad (2)$$

extending with quite satisfactory linearity over a few powers of ten. This is naturally taken as evidence of either Schottky or Poole-Frenkel emission and, since the coefficient ß for either of these is given by essentially fundamental constants, it is claimed that it should be possible to decide between the two effects from the numerical value of the coefficients. At this stage, practical difficulties arise, however, since it is not always possible to obtain a satisfactory agreement with either theory. Some authors (7) found it necessary to use unrealistically high values of the dielectric constant in order to obtain agreement with the Poole-Frenkel formula, for example value 12, which certainly appears too high for what must be taken as the high-frequency dielectric constant of silicon monoxide. Jonscher (3) in his review reported that the modification of Poole-Frenkel mechanism arised because in the present model the maximum barrier lowering $ß_{PF}E^{\frac{1}{2}}$ occurs only in one particular direction in space, all other directions having to overcome a higher barrier. The enhanced probability

$$P = \left(\frac{P_o}{R^2}\right)\int_0^R k\, e^k\, dk = \left(\frac{P_o}{R^2}\right)\left[\, e^R(R - 1) + 1\right] \qquad (3)$$

where Po is the probability of escape in any direction in the absence of field.

$$R = \frac{e\ \beta_{PF}\ E^{\frac{1}{2}}}{k\ T}$$

By contrast, the simple Poole-Frenkel model accepted normally gives

$$P_{PF} = P_o\ e^{R}\ /\ 2$$

2.2. Experimental Technique

The films were made by low pressure sputtering in a MRC 8800 system, which is described in detail in Sec. V. Prior to deposition chamber was evacuated to a pressure of the order of 10^{-6} torr. The argon gas (the purity of 99.9995%) was introduced to a pressure of 7-8 x 10^{-3} torr. The deposition rates were generally less than 55 A/min.

During deposition the substrates were in a near room temperature. Corning glass was used as a substrate and prepared by ultrasonic cleaning in Iso-propyl alcohol solution. Table I summarizes the sputtering parameters.

The test set for d-c conduction measurements employed Kepco ABC 1000 voltage source and Keithley 616 digital Electrometer. Nearly all electrical measurements were made along sputtered layers using sputtered Nb electrodes 0.4 cm apart, although a number of Nb-Ge-Nb sandwich structures

were made to investigate the current-voltage behavior at high fields.

Table 2-1 . Parameters used for the sputter depositions

Target voltage	1.6 KV
Argon pressure	5 mTorr
Substrate temperature	water cooling
Deposition time	30 min
Deposition rate	0.67 A/sec

2.3. Experimental Results and Discussion

Current versus voltage characteristics for all layers measured revealed perfectly linear and symmetric behaviour up to fields of 5 x 10^3 V/cm. The onset of non-ohmic behavior usually occured at about 1 x 10^4 V/cm. Typical graph of log I vs. log E at various Argon partial pressure are shown Fig 2-2. The non-ohmic behaviour above 10^4 V/cm

was initially observed in Nb-Ge-Nb sandwich structures.

If the results for fields greater than 10^4 V/cm are plotted in the form log I vs. $E^{\frac{1}{2}}$ straight line is obtained (Fig 2-3). This would suggest a function of the form

$$I = A \exp (\beta E^{\frac{1}{2}})$$

which is consistent with the presence of field assisted electrode emission of carriers, (Schottky effect), or internal field emission, (Poole-Frenkel effect), as observed in dielectric layers. The image force dielectric constant is obtained from the slope of Fig. 2-3 by assuming the Poole-Frenkel mechanism as

$$I = C E \exp \{ -q [\phi_o - (qE/ \epsilon_d)^{\frac{1}{2}}] / kT \} \qquad (4)$$

Here C is the proportionality constant and ϕ_o is the zero-field trap depth. The slope is 8.76×10^{-3}. Thus from $\beta_{PF} = (kT/q) \times$ slope, $\beta_{PF} = 2.25 \times 10^{-4}$. The value of dielectric constant for MIM configuration is 11.36 which is appearing to be resonable. Thus we concluded that current transport mechanism through amorphous Ge film at high fields is Poole-Frenkel mechanism and at low fields it is ohmic. When referring to power-law dependence of current upon voltage in the context of dielectric films, one naturally

tends to think of space-charge-limited flow in solids. While an ideal trap-free dielectric was known for a long time to give square-law dependence (8), other powers, for example 3/2 and also higher than 2, even as high as 5 or 6, have been observed and interpreted by Lampert (9).

It is tempting to suspect that a high-exponent power-law may be mistakenly diagnosed where, in fact, a Poole-Frenkel type law applies. But in general there should be no difficulty in distinguishing these two cases provided the data extented over a sufficient range of current. But from our data we cannot find any specific power-law depedence of current to voltage.

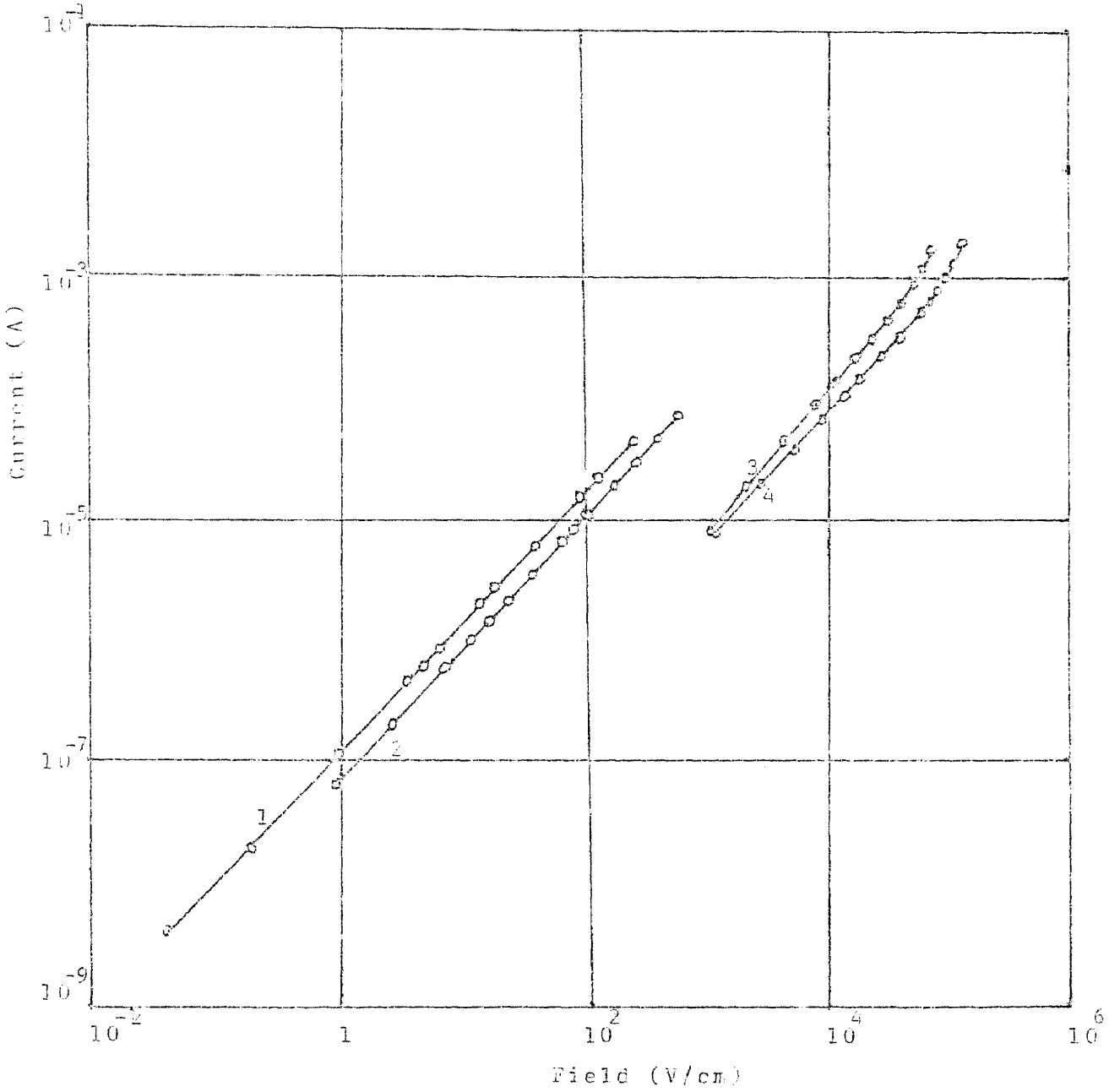

Fig. 2-2. Current-voltage characteristics for: (1),(2),samples with 0.4cm electrode separation; (3),(4),sandwich layer.

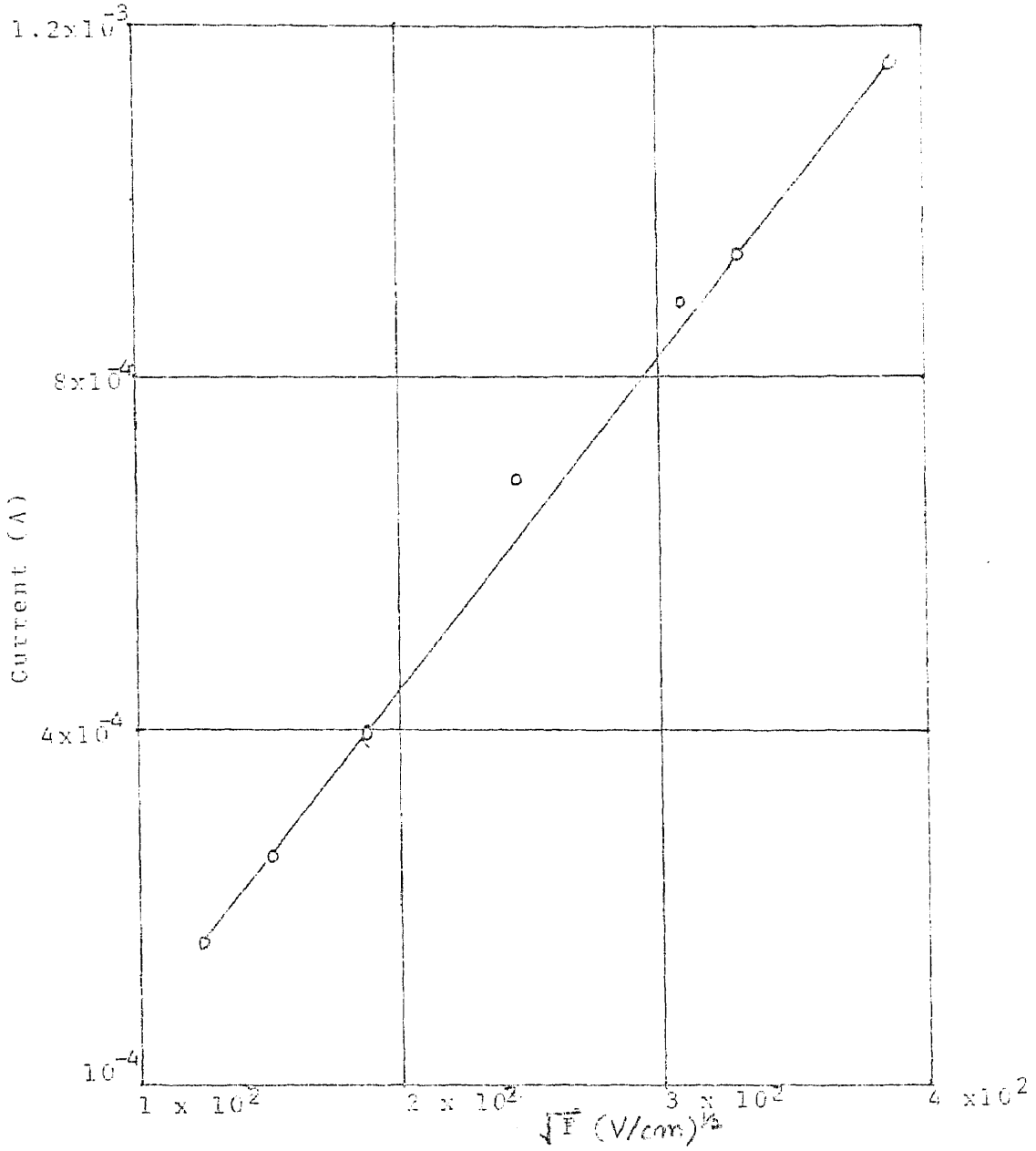

Fig. 2-3. Plot of log current vs. square root of voltage at high fields.

III. Infrared Spectra of the Ge-H Bonds in Amorphous Germanium Prepared by Bias Sputtering

3.1 Theory and background.

Pure amorphous Ge(a-Ge) or Si(a-Si) films as normally prepared by evaporation, sputtering, or ion bombardment, are quite different in terms of their optical and electrical properties from a-Ge or a-Si chemically deposited from Ge- or Si- bearing compounds, usually hydrides and, on occasion, halides. Presumably the basic difference between the "normal" and "chemical" methods is that the "normal" depositions give films permeated with paramagnetic dangling bonds of the order of 10^{20} per cm^3, as seen by electron-spin-resonance(1) and bulk-magnetic-susceptibility(2) measurements. The "chemical" methods, such as glow-discharge decomposition or reactive sputtering in hydrogen(3), give films with considerably lower concentrations of paramagnetic dangling bonds, less than 10^{16} cm^{-3} in some cases. The dangling bonds are presumably saturated by hydrogen atoms introduced into the film during preparation.

The presumption has not always been accepted for a-Si produced from glow discharges of silane. Early infrared(IR) studies did not show any bonded hydrogen(4) and later such evidence was found only in films prepared below 400 K.

However, we feel that the bulk of the evidence is that hydrogen is indeed responsible for the passivation of dangling bonds and the concomitant changes in optical and electrical properties. For example, hydrogen can be added during sputtering depositions of a-Ge or a-Si to reproduce the key doping results(5,6) previously attained only with glow-discharge produced films(7,8).

We report here measurements and identification of IR-active vibrations in hydrogenated a-Ge films. Results are given for a a-Ge films prepared by depositions from a germanium target sputtered with hydrogen-argon mixtures. From the vibrational spectra we are able to identify a variety of hydrogen bonding sites corresponding to isolated GeH bonds as well as GeH_2 and GeH_3 groupings.

3.2 Experimental Procedures.

A variety of amorphous hydrogenated germanium films were prepared in a reactive sputtering deposition system. This system is a biased rf diode system for reactive sputtering depositions in hydrogen mixtures from a germanium target. Some samples were prepared by conventional rf diode system to compare IR spectra with bias sputtered films.

The rf bias sputtering apparatus is shown schematically in Fig. 5-2. The cathode target is nominally intrinsic single crystal germanium which is bonded to a water-cooled

stainless steel plate. All deposits were made onto room temperature substrates. Before sputtering, the chamber is evacuated to less than 2 x 10^{-6} Torr. The sputtering mixture is obtained by first adjusting the H_2 flow to the desired indicated partial pressure with an ion gauge; then the Ar flow in adjusted to give a total indicated pressure. Table 3-1 summarizes the sputtering parameters. The a-Ge:H films were deposited through metal masks onto silicon substrates. For IR transmission measurement, we generally used n-type, high resistivity(70-90 ohm-cm) Si wafers polished on one side.

Table 3-1.

Target Voltage	2000 V
Total Pressure	6 - 8 mTorr
Applied Substrate Bias	100 - 150 V
Deposition time	15 min
Accumulation rate	0.9 A/sec

All spectra reported here were measured at room temperature. Most of the transmission data was measured in the ir region from 2.5 to 50 μm (4000 to 2000 cm^{-1}) with a Perkin-Elmer model 457 double beam spectrophotometer (Appendix A). All the transmission measurements were made

relative to an uncoated reference Si substrate.

3.3 Results and Discussion

Three groups of structures are expected for the variation spectra of Ge-H bonds: stretching (w^S), bending (w^B), and wagging or rocking (w^W,w^R), corresponding to the three rows of modes shown in Fig 3-1(9). The bending modes are due to the forces opposing changes in the angles between Ge-H bonds with GeH_2 or GeH_3 groups. Contrary to the stretching and wagging vibrations, the bending modes should be absent for Ge atoms bonded to a single H, i.e., isolated GeH groups. Thus a measurement of the ratio of the ir absorption strength of the bending to the stretching modes should give and indication of how much of the H is bonded to Ge as isolated H atoms. It is also known that the frequency of the stretching vibrations decreases slightly in going from triple H groups (w_3^S) to single hydrogens (w_1^S)(10). Connell and Pawlik (3) reported that a comparison of their absorption spectra of GeH with the spectra of gaseous GeH_4 and GeD_4, liquid $GeBr_3H$, and $GeCl_3D$, indicated that the local Ge-H and Ge-D bond bending (0.07 and 0.0515 eV, respectively) and bond stretching (0.23 and 0.165 eV, respectively) modes were observed rather than new electronic transitions.

Rudder et. al(11) observed that the hydrogenated

germanium films prepared by magnetron sputtering were shown the peak at 2000 cm^{-1} due to GeH_2 bond-stretching vibrations and the peak at 1880 cm^{-1} due to GeH bond-stretching vibrations and the peak 570 cm^{-1} due to GeH_2 bond-bending vibrations.

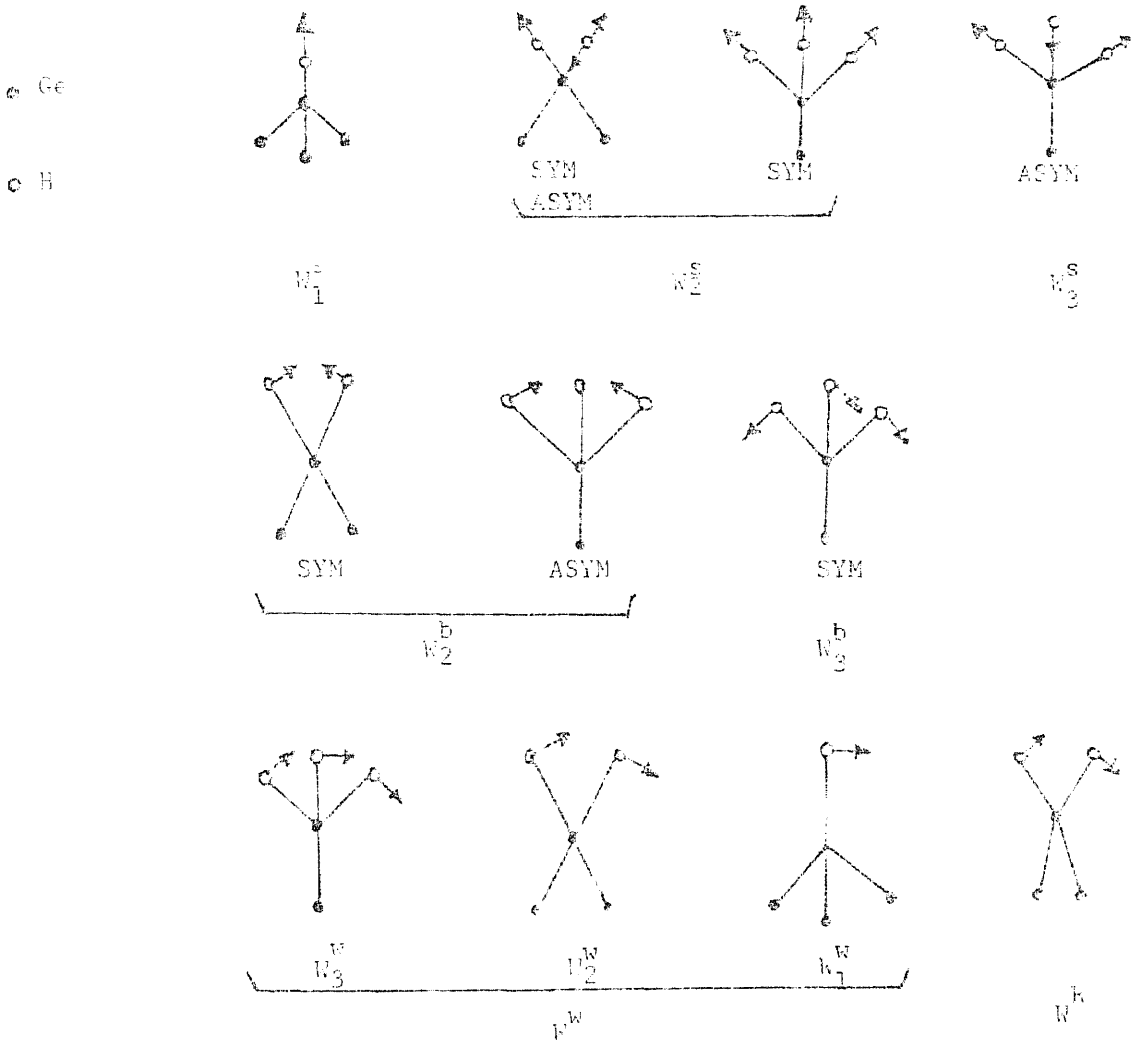

Fig. 3-1. Schematic illustration of the bond-streching (top row), bond-bending (middle row), and bond wagging and rocking(bottom row).

Table 3-2 contains the growth parameters for six films on which all the characterization has been performed. The ir spectra for these films are shown in Fig. 3-2 and Fig 3-3.

It is clear from Fig. 3-2 that increaing hydrogen partial pressure give more absorption strength of GeH_2 bond-stretching at 1950 cm^{-1}. Increasing hydrogen partial pressure also give more absorption peak of GeH bond-stretching at 1880 cm^{-1}, but it seems to be saturated at certain amount of hydrogen partial pressure (> 1 x 10^{-3}).

Table 3-2

Growth Parameters			Peak frequencies	
Sample number	Method	Hydrogen Pressure($x10^{-3}$)	Stretch bands	Bend bands
H4	bias	0.4	1880	590
H3	bias	0.6	1890	570
H2B	bias	2	1880	590
H1B	diode	1	-	-
H6	bias	0.8	1880(1680)	-
H5	bias	0.8	1880(1680)	-

The IR spectra of all the samples except two are qualitatively similar to those shown in Fig. 3-2. The exceptions are shown in Fig. 3-3 which have the absorption peak at 1680 cm^{-1}. According to Connell and Pawlik(3), The vibrational modes $Ge_{1-x}H_{0.5x}D_{0.5x}$ appeared to be a superposition of the mode in $Ge_{1-x}H_x$ (1880 cm^{-1}) and $Ge_{1-x}D_x$ (1350 cm^{-1}). Therefore, the films in Fig. 3-3 can be assumed to be $Ge_{1-x}H_{0.5x}D_{0.5x}$.

In summary, we have grown amorphous germanium films that have same GeH and GeH_2 stretching vibration mode but much smaller absorption strength at bending vibration mode than the result reported previously . The important question of why these films are different from those grown by glow discharge or magnetron sputtering methods cannot be answered from the limited studies presented here. We believe that it is at least related to the chemical purity of the films and the control of substrate temperature. We are undertaking further studies to try to better understand the importance of the various growth parameters on the properties of bias sputtered hydrogenated amorphous films and to determine what differentiates their properties from films produced by other techniques.

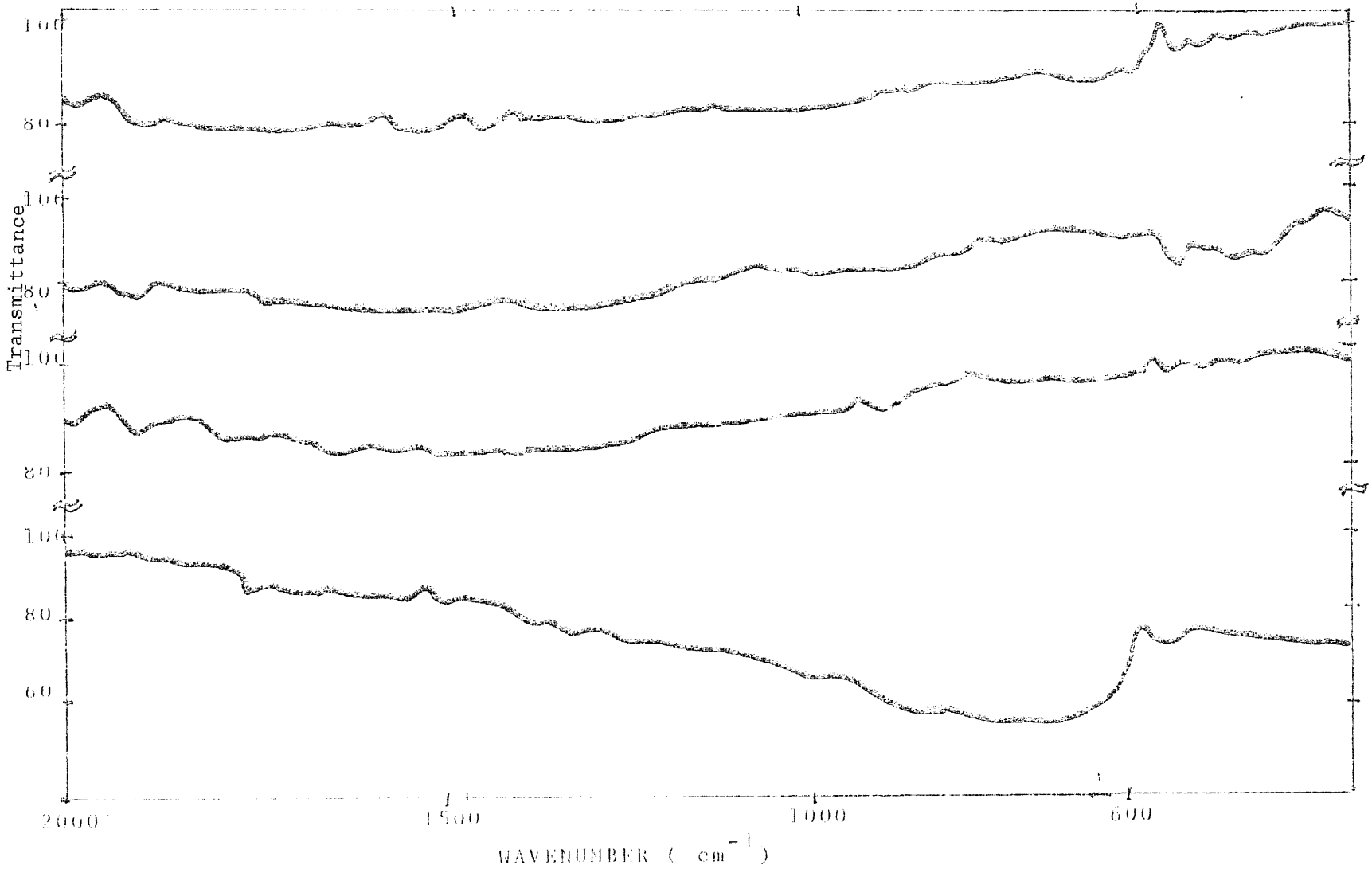

Figure 3-2. IR spectra for Ge:H samples.

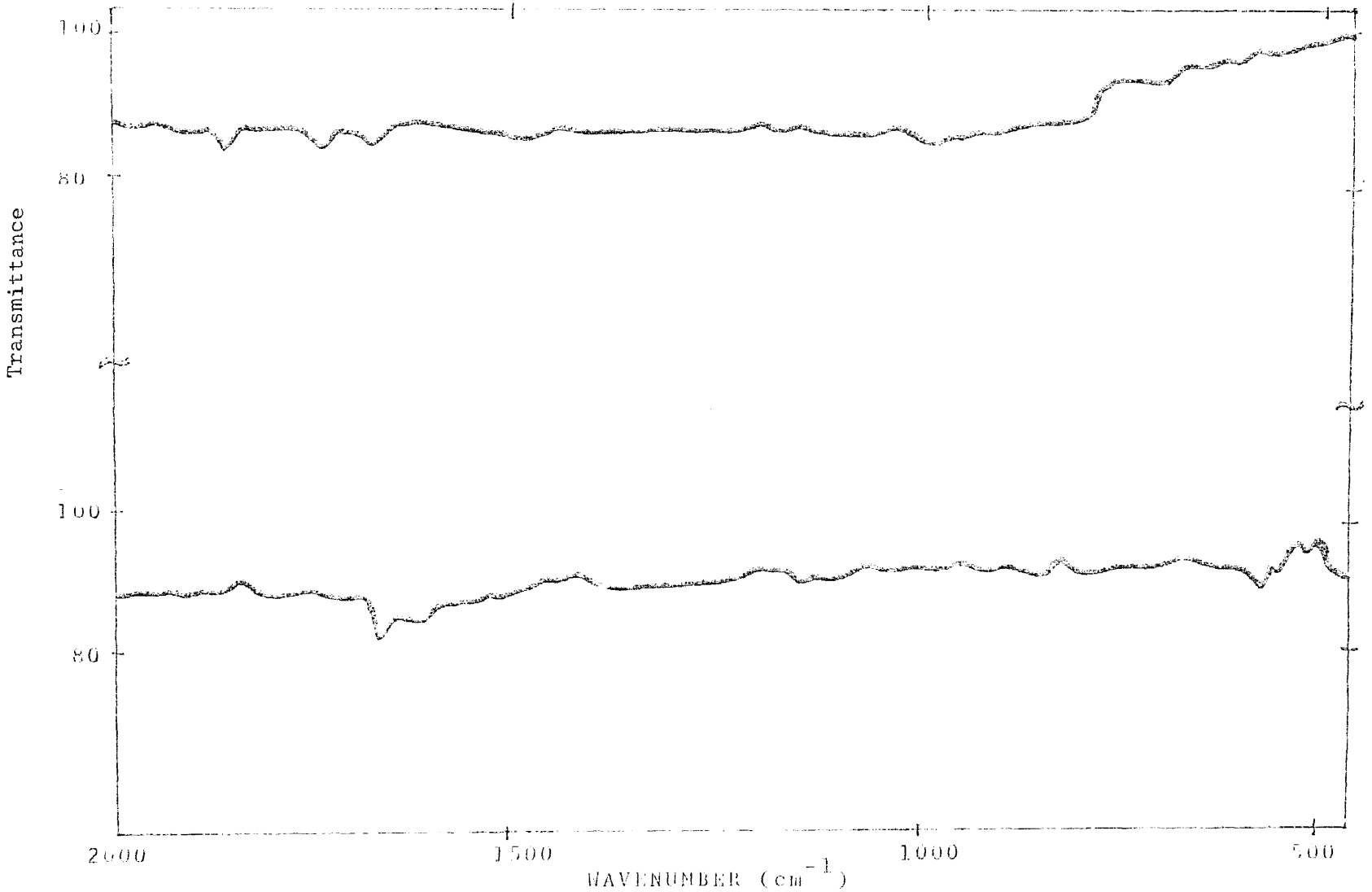

Figure 3 - 3. IR spectra for $Ge_{1-x}H_{0.5x}D_{0.5x}$ samples.

IV. Determination of optical constants from transmittances over an absorption band using dispersion relations.

4.1 Theory and Background

It is well known that when an electromagnetic wave is transmitted, the transmittivity and accompanying phase shift are not entirely independent quantities. For example, the phase shift at any one frequency can be expressed as an integral involving the transmittivity at all frequencies. The calculation of the phase shift in this manner was discussed by Simon (1), and was later generalized and applied by Robinson and Price (2). The practical application of the dispersion relation to obtain the phase shift from the transmittivity involves certain difficulties. Although with a digital computer the numerical integration is not a serious problem, a more fundamental difficulty arises because the integrations run from zero frequency to infinity whereas the required transmittivity data are available only for a limited frequency range. This lack of data over the entire region of integration can lead to very serious errors. Schatz et al. (3) outlined a procedure to be used with a digital computer which seems to be very successful in handling this problem. From the phase shift and the transmittances, the refractive index and absorption

coefficient can be then calculated at each frequency over the band.

A. Kramers-Kronig Dispersion Relation

A beam of incident intensity Io impinges at normal incidence on a film of thickness d and optical constants n(v) and k(v), which is deposited on the front of a thick window of refractive index Ø. R_i designates the fraction of a light beam travelling to the left in the window medium which would be reflected at the interface with the deposited sample.

$$I = Io\ Ø\ T_2\ (1 - R_w)\ (1 - R_w\ R_i)^{-1} \qquad (1)$$

where $$T = \frac{t_1\ t_2\ \exp\ (ir)}{1 + r_1\ r_2\ \exp\ (2ir)} \qquad (2)$$

and

$$t_1 = 2\ (\ 1 + n)^{-1} \qquad t_2 = 2\ n\ (n + Ø)^{-1}$$

$$r_1 = (1 - n)\ (1 + n)^{-1} \qquad r_2 = (n - Ø)(n + Ø)^{-1}$$

$$r = 2\ \pi\ n\ d\ v$$

N is the complex refractive index, and the true absorption coefficient $A = 4\ \pi\ k\ v$ where 1/v is the wavelength in air.

$$R_w = (Ø - 1)^2\ /\ (Ø + 1)^2$$

and Ri is given by (5,7)

$$Ri = \frac{(g_2^2 + h_2^2)e^{\beta} + (g_1^2 + h_1^2)e^{-\beta} + E \cos m - B \sin m}{e^{\beta} + Q\, e^{-\beta} + C \cos m + D \sin m} \qquad (3)$$

$$\beta = A\, d = 4\, \pi\, k\, v\, d$$

$$m = 4\, \pi\, n\, v\, d$$

$$B = 2\,(g_1\, h_2 - g_2\, h_1)$$

$$C = 2\,(g_1\, g_2 - h_1\, h_2)$$

$$D = 2\,(g_1\, h_2 + g_2\, h_1)$$

$$E = 2\,(g_1\, g_2 + h_1\, h_2)$$

$$g_1 = \frac{Q^2 - (n^2 + k^2)}{(n + Q)^2 + k^2}$$

$$h_1 = \frac{2\, Q\, k}{(n + Q)^2 + k^2}$$

$$g_2 = \frac{(n^2 + k^2) - \emptyset^2}{(n + \emptyset)^2 + k^2}$$

$$h_2 = \frac{-2\, \emptyset\, k}{(n + \emptyset)^2 + k^2}$$

The expression $Io\emptyset|T|^2$ represents the intensity of the incident beam after it was entered the window medium. The factor (1-Rw) represents the fraction of this beam transmitted into the air through the back of the window on the first pass, and the factor $(1-RwRi)^{-1}$ takes account of the multiple reflections arising from the presence of the

last window air interface.

We have assumed that the sample and window faces are flat, parallel, and nonscattering. We note that the transmittance of the incident radiation through the film does not obey Beer's law except in the limit of large (d v) when interference and multiple reflection effects become unimportant.

Noting from Eq.(2) that T is a complex quantity, we write

$$T = |T| \exp (iQ) \tag{4}$$

$$\text{or} \quad \ln T = \ln |T| + iQ \tag{5}$$

where $i = \sqrt{-1}$ and Q is phase shift. Kramers-Kronig type dispersion relation relates |T| and Q (4),

$$Q(\nu_o) = \frac{-2\,\nu_o}{\pi} P\int_o^{\infty} \frac{\ln |T(\nu)|\, d\nu}{\nu^2 - \nu_o^2} + 2\pi\nu_o d \tag{6}$$

where v is expressed in cm^{-1} and P signifies the principal value of the integral. |T| and Q in turn are related to n and k as follows;

$$|T| = 4\,[(n^2 + k^2) / (C^2 + D^2)]^{\frac{1}{2}} \tag{7}$$

$$Q = \arctan [(kC + nD)/(nC-kD)] \tag{8}$$

where

$$C = e^{M}[P \cos N + Q \sin N] + e^{-M}[L \cos N - H \sin N]$$

$$D = e^{M}[P \sin N - Q \cos N] - e^{-M}[L \sin N + H \cos N]$$

and

$$P = (1 + n)(n + \emptyset) - k^2$$

$$L = (1 - n)(n - \emptyset) + k^2$$

$$Q = k(1 + 2n + \emptyset) \qquad H = k(1 - 2n + \emptyset)$$

$$N = 2\pi v n d \qquad M = 2\pi v k d$$

Hence if Q can be evaluated from Eq. (6) at each frequency, |T| and Q can be used to evaluate n and k at each frequency through Eq. (6) and Eq. (7).

4.2 Application of the theory

First, we must determine |T| from Eq. (1). In practice, it is usually convenient to use Io' rather than Io for the base line, where Io' is the transmittance of the blank window. In this case, we find that

$$|T|^2 = (I/Io'\emptyset)\left[(1 - RiRw)/(1 + Rw)\right] \qquad (9)$$

Since Ri is a function of n and k (which we have not yet calculated), we calculate |T| from Eq.(9) using experimental (I/Io) data assuming Io a first approximation that

$$(1 - RiRw) / (1 + Rw) = 1 - Rw \qquad (10)$$

Let us designate V_L and V_R as the low and high frequency ends, respectively, of the absorption region under consideration. It is essential that these two points be sufficiently far from the absorption maximum that we can assume k=0 without apprecable error.

Designating n_L and n_R are the refractive indices of the film at v_L and v_R, we can calculate n_L and n_R from Eq.(7) (k=0). Using these values of n_L and n_R, we calculate Ri at v_L and v_R from exact expression for Ri (k=0) (Eq.(3)). Using these values of Ri and Eq(9), we recalculate $|T|$ at v_L and v_R ($|T_L|$ and $|T_R|$), we then repeat this process, if necessary, until self-consistency is achieved. This occurs quickly because Ri enters only as small correction. If, as a first approximation, we assume that the transmittance from 0 to v_L has the constant value $|T_L|$ and that the transmittance from v_R to ∞ has the constant value $|T_R|$, we can compute Q at each frequency in the interval v_L to v_R by means of Eq. (6). The integral between v_L and v_R must of course be done numerically using transmittance data [but with the approximation expressed by Eq. (10)]. The following is the digital computer procedure (3) for doing this. The integrations between 0 and v_L and between v_L and infinity are elementary. The integration between v_L and v_R must be done numerically. we divide the region from v_L to

v_R into L equal intervals of increment h. we then fit the experimental ln |T| curve at each set of three successive points by a parabolic arc,i.e,

$$\ln |T| = a + b\, v + c\, v^2 \qquad (11)$$

Thus for the interval between v_K and v_K+2h, a, b, and c would be determined from the measured values of ln |T| at v_K, v_K+h, v_K+2h. Substituting Eq. (11) into Eq. (6) yields integrals which can be evaluated analytically in all cases.

$$Q\,(v_o) = -\frac{\ln|T_L|}{\pi} \ln \frac{n\,h}{2\,v_L + n\,h} - \frac{\ln|T_R|}{\pi} \ln \frac{[2v_L + (1+n)h]}{(1-n)\,h}$$

$$- \frac{2\,v_o}{\pi} \int_{v_L}^{v_R} \frac{\ln|T(v)|\,dv}{v^2 - v_o^2} + 2\,\pi\, v_o\, d \qquad (12)$$

It is clear that the phase shift calculated in the manner just described is quite unsatisfactory. This is a consequence out of simplified treatment of the frequency regions outside the absorption band (0 to v_L and v_R to infinity). The critical requirement for the success of our method is a reliable general procedure for correcting the initial result. Starting with the values of n_L and n_R obtained previously, we calculate values of Q at v_L and v_R (Q'_L and Q'_R) using Eq. (8) (k=0). we now raise the broken curve in such a way the extreme left hand point (Q_L) is

brought into coincidence with Q'_L, the extreme right hand point (Q_R) is brought into coincedence with Q'_R, and the points in between are raised proportionately (6);

$$\frac{v_R - v}{v_R - v_L}(Q'_L - Q_L) + \frac{v - v_L}{v_R - v_L}(Q'_R - Q_R)$$

Using this new Q curve and experimental transmittances |T|, we calculate n and k at each frequency throughout the band from Eq. (7) and (8). This can be done very conveniently by a methods of successive approximation using a digital computer by Newton's method. |T| and Q are first calculated using trial values for n and k. The calculated |T| and Q are compared with the actual |T| and Q and n,k are corrected on the basis of comparisons. The procedure is repeated until the calculated |T| and Q agree with the actual |T| and Q to any specified degree of accuracy. This procedure can be made to converge very quickly by making use of the explicit functional relations between n and k and |T| and Q. Thus by working out the partial derivatives of |T| and Q with respect to n and k, straight forward algebraic expressions can be obtained for the first order corrections to n and k for each successive cycle. When the program moves to the next frequency point, the final values of n and k obtained for the previous frequency are used as a first approximation.

Since n and k values are now available, we may go back

and calculate Ri at each frequency from the exact formula rather than resorting to the approximation expressed by Eq. (9). With these Ri values, we then recalculate |T| from Eq. (9), and repeat the previous procedure to obtain improved values of Q, n, k. (we also improve the previous calculation of n_L and n_R by using values for k_L and k_R in Eq. (9) rather than assuming k=0.

In practice, it will very often happen that the method described for determining n_L and n_R will be inadequate because n_L and n_R have been calculated directly from experimental transmittance data. For such a calculation to accurate, it is necessary that the transmittance be measured very accurately, that there be no light scattering, and that the system generally behave ideally.

4.3 Results and discussion

The optical constants of a-Ge:H films were determined by using this method. The results, however, turned out to be poor. For example, the dielectric constant(= n^2 at k = 0 region) came out to be 25 which is not a reasonable value. The poorness of results can be explained by two possible facts; i) the absorption peak of a-Ge:H films happened to be in the transition region of changing filters of our infrared spectrophotometer. Therefore the transmittance data set cannot be determined exactly. ii) Small size of

Ge target(2 1/4") gave non-uniformity of a-Ge:H film thickness because the size of target greatly influence on the uniformity of film thickness.

Instead of a-Ge:H films, silicon nitride films were used because silicon nitride film does not have bad aspects of a-Ge:H film stated above. Fig. 4-1 and Fig. 4-2 show the results of an application of our method to an experimental data of silicon nitride in the range of 350 - 1430 cm^{-1}. Silicon nitride film was deposited onto silicon substrate by direct sputtering in our system. The refractive index of silicon substrate is 3.42. The thickness of silicon nitride film is 1700 A. The transmittance in Fig. 4-3 is normalized to the absorption-free background transmittances in order to eliminate the shallow interference fringes due to the small index of refraction difference between the substrate and the film. We can convert the transmittances to absorption coefficients by

$$A = 4 \pi k v$$

where k is the extinction coefficient which is determined by our program and v wavenumber. These absorption coefficients is compared in Fig. 4-4 with the values calculated by

$$A = -\ln (I/Io) / t$$

where t is the film thickness.

Since refractive indicies have been calculated directly from experimental transmittance data, it is necessary to check the correctness. The dielectric constant of silicon nitride in the region k=0 is about 6.5(= n^2) which is consistent with the dielectric constant calculated by I-V characteristics.

It is concluded that the optical constants n and k can be calculated from transmittance data and absorption coefficient can be determined exactly using calculated extinction coefficient.

In our treatment, we have not attempted correct for an light scattering. The total computer time used was about 10 min with Convergence Technology minicomputer.

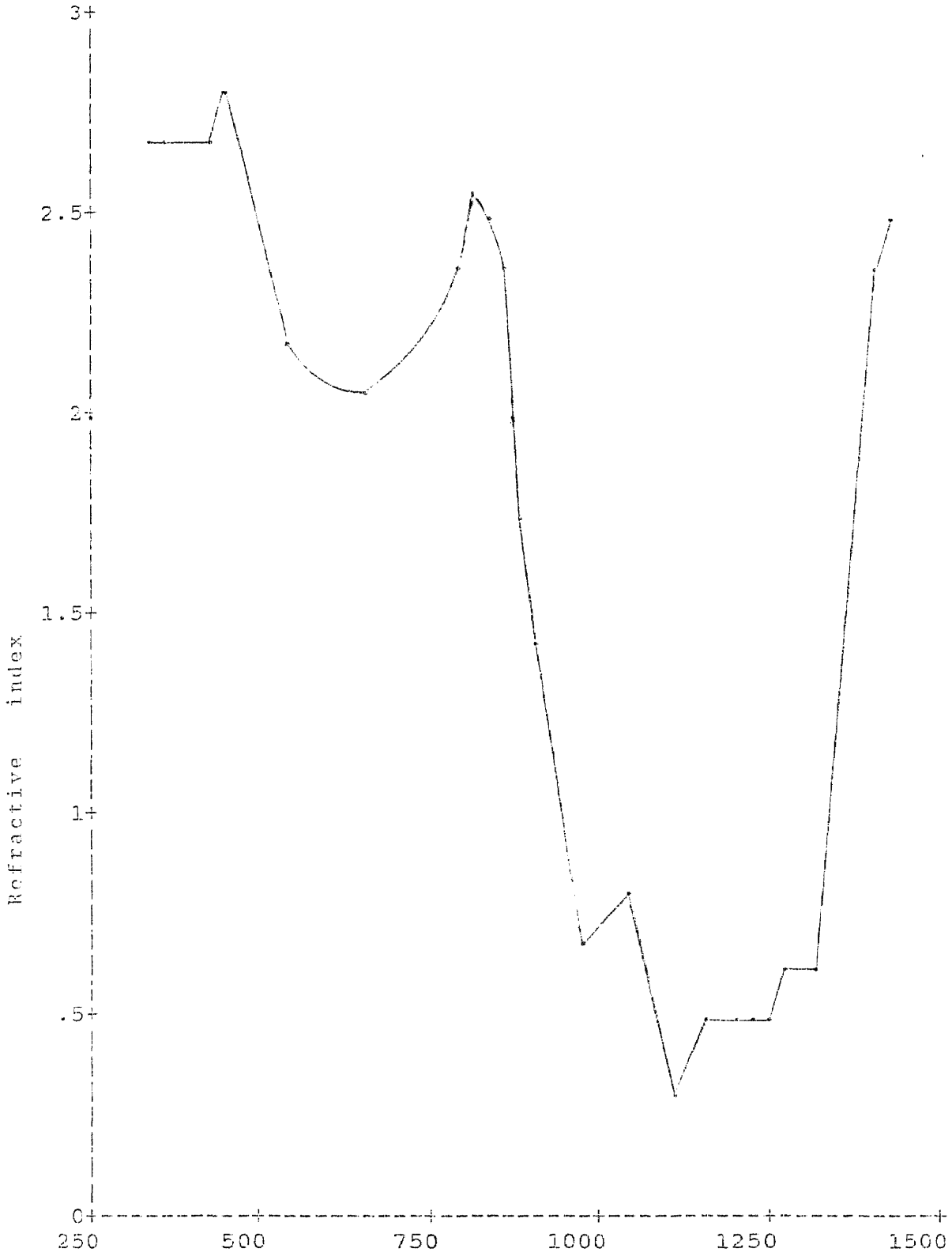

Figure 4-1. Calculated refractive index of solid Si_3N_4 as a function of frequency.

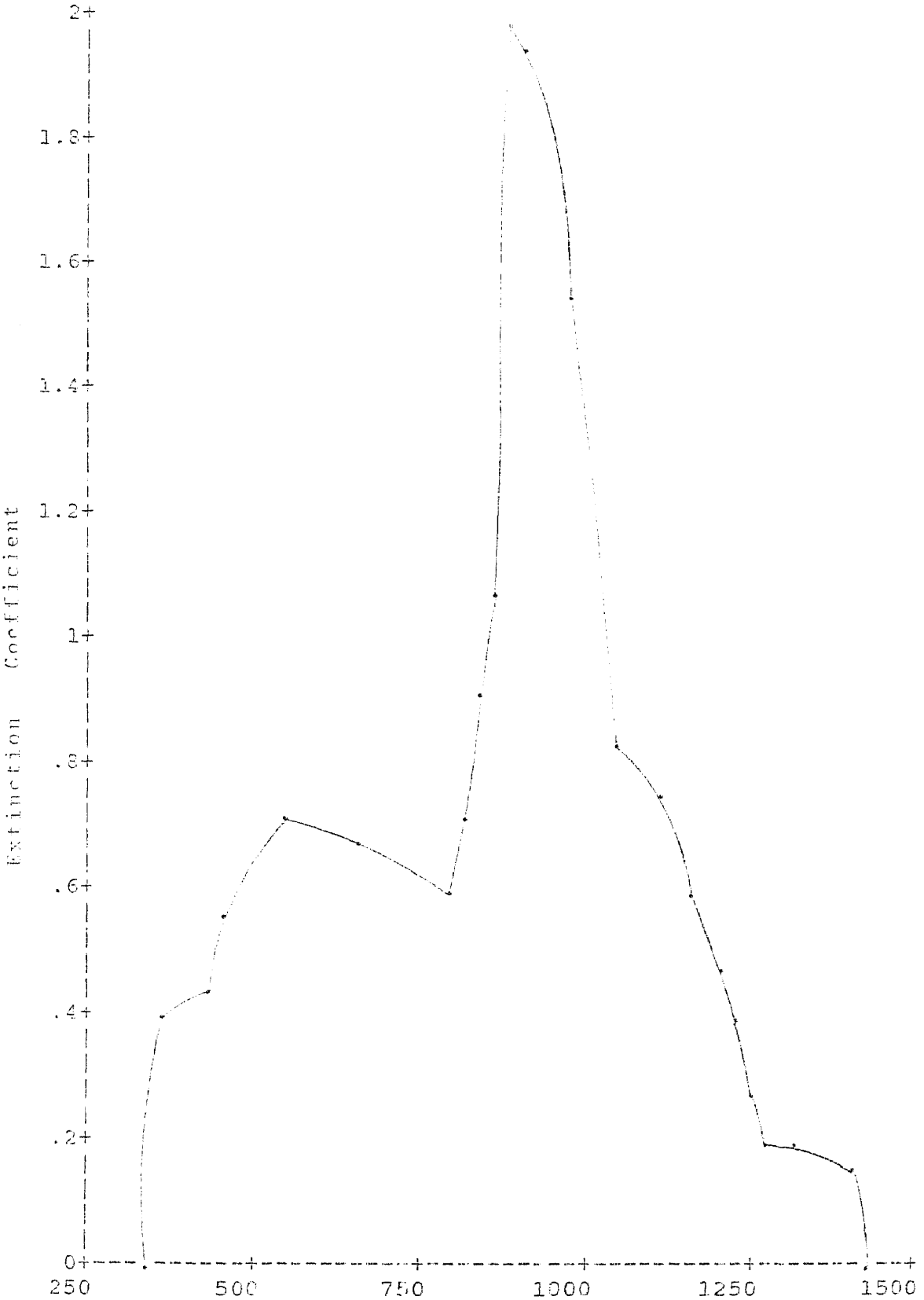

Figure 4-2. Calculated extinction coefficient of solid Si_3N_4 as a function of frequency.

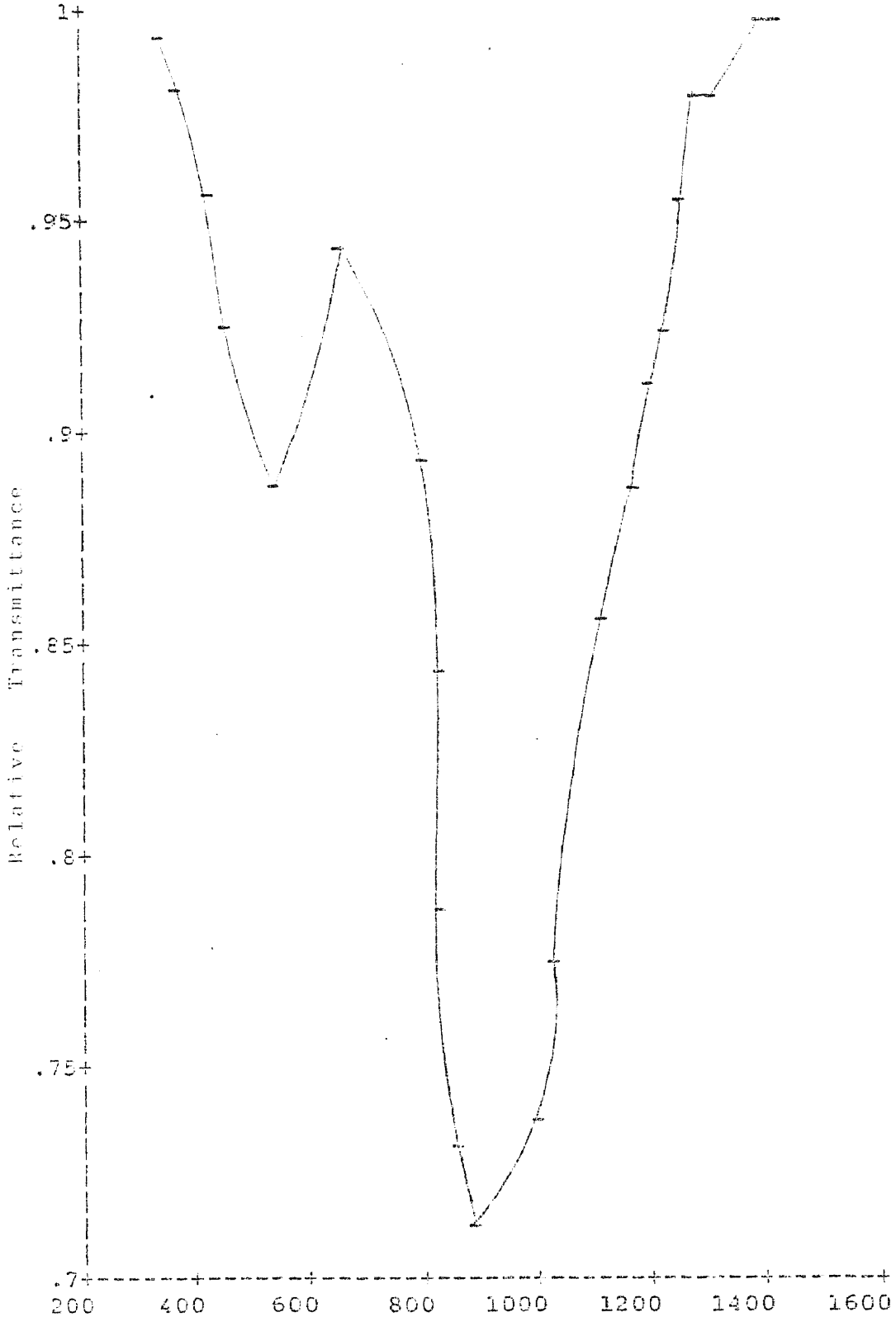

Figure 4-3. Representative transmittance T versus frequency of ir spectra for Si_3N_4 film. The transmittance is shown relative to the absorption-free background transmittance of the same film.

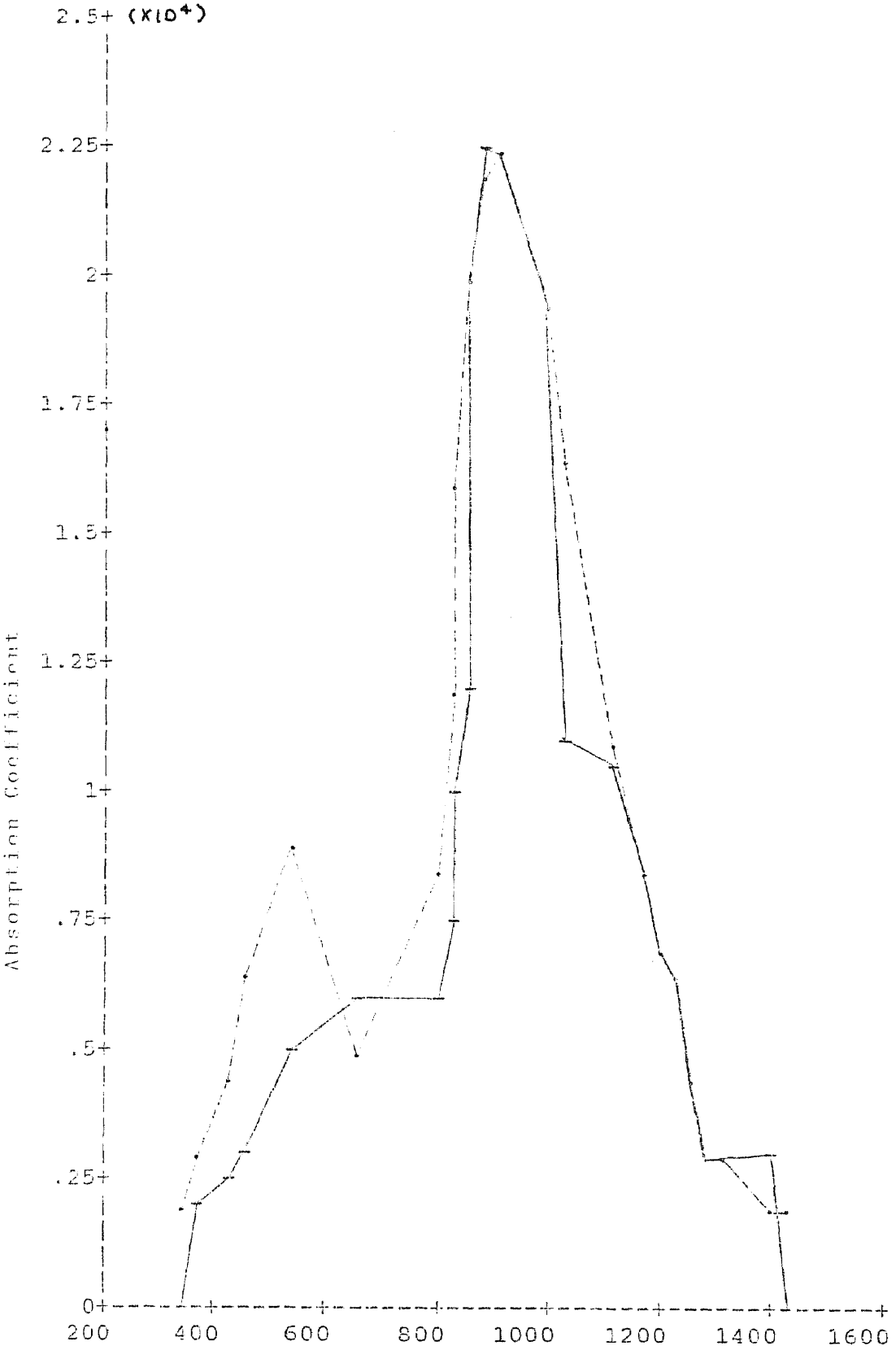

Figure 4-4. Absorption coefficient of solid Si_3N_4(on Si) as a function of frequency. The solid line is the calculated true value and the broken line is the experimental curve.

V. SPUTTERING

5.1 THEORY

A. What is sputtering

Deposition of thin films by sputtering involves the acceleration of positive ions from a gaseous plasma through an electron free region (Langmuir Sheath) to bombard a target material that is negatively-charged due to the application of either a dc or rf (13.56 MHZ) voltage. The surface atoms (within about the first five layers) are

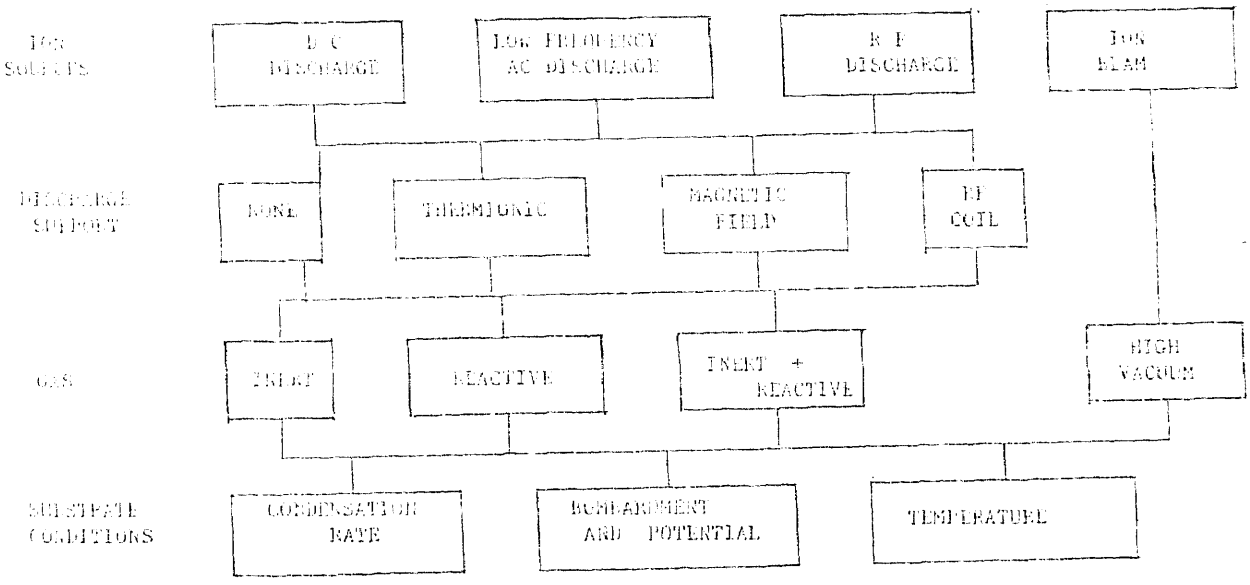

FIG. 5 - 1. SPUTTERING PROCESSES (7)

ejected by momentum transfer and after transversing the plasma region arrive with relatively high energies at the substrate. These ejected atoms, which can also be charged and in some cases, molecular species, deposit at the substrate and are largely incorporated into the growing film.

The versatility of sputtering process often allows on to tailor film properties in ways not always available with other methods of film deposition. This versatility arises because of the many possible permutation and combinations of process conditions. Fig. 5-1 is a kind of organization chart for sputtering process which graphically illustrates most of the possibilities.

B. Various Effects of Sputtering

Next is a brief review of some effects that occur at the target, in the gas discharge, and at the substrate.

1. Physical and Chemical Effects at Target Surface

When a solid surface is bombarded by energetic ions, numerous effects may occur: i) emission of neutral (sputtered) particles; (ii) emission of secondary electrons; (iii) emission of positive and/or negative ions; (iv) emission of radiation; (v) reflection of incident particles; (vi) desorption of gases; (vii) implantation of incident particles;

(viii) heating; (ix) chemical dissociation; (x) bulk diffusion; (xi) crystallographic changes; and (xii) reflection of some emitted species back to the target surface either by collision in the gas discharge of electrostatic attraction. Since the target is held at high negative potential, secondary electrons are emitted at target potential and accelerated toward the substrate. Upon arrival, such energy as they retain after colliding with sputtering gas atoms is liberated at the substrate in the form of heat.

It is highly improbable that a positive target ion generated at the target surface could escape the negative field tat that surface. Honig (1) has shown that hte fraction of positive ions originating at the target surface that escape the target field is very small (<1%) and the escape mechanism is very complex. The number of positive ions that are produced and, hence, can escape, is larger for compounds than for monatomic targets. Benninghoven (2) has shown that this occurs because of dissociation reactions in which the primary bombardment breaks down molecules into positive and negative ions that are then sputtered. He showed that the number of positive and negative ions released from metal targets decreases to a negligible minimum as the surface oxides on the target are sputtered away. Negative ions produced by dissociation reactions are repelled from the target and accelerated toward the substrate. The ions may be neutralized by stripping collisions in the gas.

2. Occurrences in the Gas Discharge

We have noted above that numerous energetic particles (electrons, ions, and neutrals) are liberated from the target and propelled toward the substrates. If bombardment by these particles is undesirable, a high gas pressure can aid in slowing these particles to minimize substrate heationg and other effects to be described. In some cases it will be desirable to maximize the bombardment, thus dictating the use of low gas pressure.

It was shown above that the likelihood of a positive target ion escaping the target field is very small. However, it is entirely possible to create positive target ions by collisions in the rf glow discharge. This is less a problem in dc- than in rf-glow discharges because of the higher ionization probability in the latter.

The probability that ions so produced would be neutralized before arriving at the substrate is very small. Positive ions and electrons recombine more readily at solid surfaces than in the gas discharge because both momentum and energy can be conserved with greater ease in a three-body collision (ion,electron, surface) than in a two-body collision (ion, electron). Hence, ions of target material produced in this manner may bombard the substrate surface, or, in some cases, return to the target to cause self-sputtering.

3. Effects Occuring at Substrates

There are three basic effects that occur at substrate surfaces during rf sputtering. Material from the target arrives at the substrate surface and condenses from an excited state; the substrates are subjected to bombardment by various energetic species; and the substrates are heated.

C. Bias Sputtering

The term bias sputtering refers to the purposeful bombardment by energetic ions of a growing film. There are numerous techniques by which this has been accomplished in the past. Asummetric ac sputtering was the first such technique introduced. This technique utilized a low-frequency ac discharge in which the positive portion of the target signal is attenuated. At the substrate, the reverse is true, giving rise to a small negative potential on the substrate during half the period of the waveform. Maissel and Schaible (3) used dc sputtering with dc-substrate bias applied to the substrate surface by way of clips. Mattox (4) introduced a system which he called ion plating. This technique involves thermal evaporation onto a surface that is being dc sputter etched. Vossen (5) reported on a system that utilized dc sputtering as the deposition source with an rf-induced substrate bias. Later Logan (6) descri-

bed a system in which it was possible to rf sputter onto a surface with an rf-induced substrate bias (Appendix B). In his technique, rf power is coupled to the substrate holder through the rf discharge.

5.2 SPUTTERING SYSTEM IN N.J.I.T

A. Description of Sputtering System

MRC 8800 sputtering system in Fig. 5-2 is composed of

1. RF power generator
2. D.C power generator
3. Main chamber and intervac chamber
4. Pressure gauge
5. Cryogenic pump
6. 2 rotary pumps
7. Target tuning box
8. Anode bias tuning panel

R.F power generator has maximum ouput 2000 W at 13.56 MHZ. High-pressure ionization gauge controller and tube of Granville-Phillips Co. is used to measure the gas pressure of the main chamber.

The main chamber has four targets, anode, and plasma confinement box inside. The rotational turret having gour

targets is a metallic cubic structure. Different targets are fixed on each of four faces of the cube and shafts, holding this cube in position, are attached to other two faces. Shaft connected to target tuning box also carries water lines which is designed to carry rf voltage too. In triode sputtering, a tungsten wire filament is heated to a temperature sufficient to supply electrons by passing an adjustable alternating current through it. The electrons are attached to the anode by a positive voltage. These electrons will collide with some of the gas atoms knocking off electrons and leaving the atoms positively charged. As the gas pressure and/or the anode voltage is increased, more and more collision will occur until a visible plasma can be seen. The filament and the anode are enclosed in water cooled boxes with a plasma box coupling them together. This box serves to confine the plasma and to prevent any material evaporated from the filament reaching the substrates of target face.

The intervac chamber and its associated pumping system allow substrates to be introduced into the sputtering chamber without venting main chamber to atmosphere.

The procedure of pumping out main chamber is
i) decrease the pressure in the chamber below 100 militorr by mechnical pump ii) open the high-vaccum value connected to cryogenic pump. Cryogenic pump, Cryo-Torr 8 of the CTI-cryogenic, is used to pump the main chamber out to 10 Torr.

Cryogenic pump has no moving parts, operating fluids or backing pump, exposed to the volume to be pumped, which totally elliminates possibility of contamination. The major disadvantage associated with cryopumps is that they are capture pumps as opposed to throughout pumps. This means all gases pumped are retained within the system and eventually build up enough to affect the pump's performance. This requires a periodic regeneration cycle where the pump is warmed up to room temperature to enable the trapped gases to be released. In our system, the regeneration cycle is about 2 months.

B. The sputtering procedure

1. Turn on rf power generator, A.C. filament power supply, and D.C. filament power supply.
2. Adjust filament current slowly to 50 amps and D.C. vo lts 100 V which usually take 3-4 min.
3. Adjust desired hydrogen pressure and allow argon about 10 militorr. Because of cryogenic pump's limited capa city the hydrogen pressure should be under 1x10 Torr. Experimentally if the hydrogen partial pressure is more than 1 militorr the temperature of cryogenic pump starts to rise, then the main system has to be turned off. If the temperature keeps on rising, the cryogenic pump has to be regenerated.

4. Turn rf supply on and increase the argon pressure slowly until plasma is made. After plasma is made, reduce the argon pressure to the desired pressure.
5. Adjust the input tuning and the load tuning of target tuning box to make reflected power as low as possible. The forward power should be less than 250 - 300 W. If it goes over this range, the breaking of the pyrex which covers backside of target can be resulted. In bias sputtering, anode input tuning and output tuning is adjusted simultaneously to get a desired substrate bias. Experimentally the following tuning procedure for bias sputtering is recommended:
    i) Adjust forward power properly using the target load tuning.
    ii) Reduce reflected power by adjusting the target input tuning.
    iii) Set the desired bias voltage by the anode load tuning.

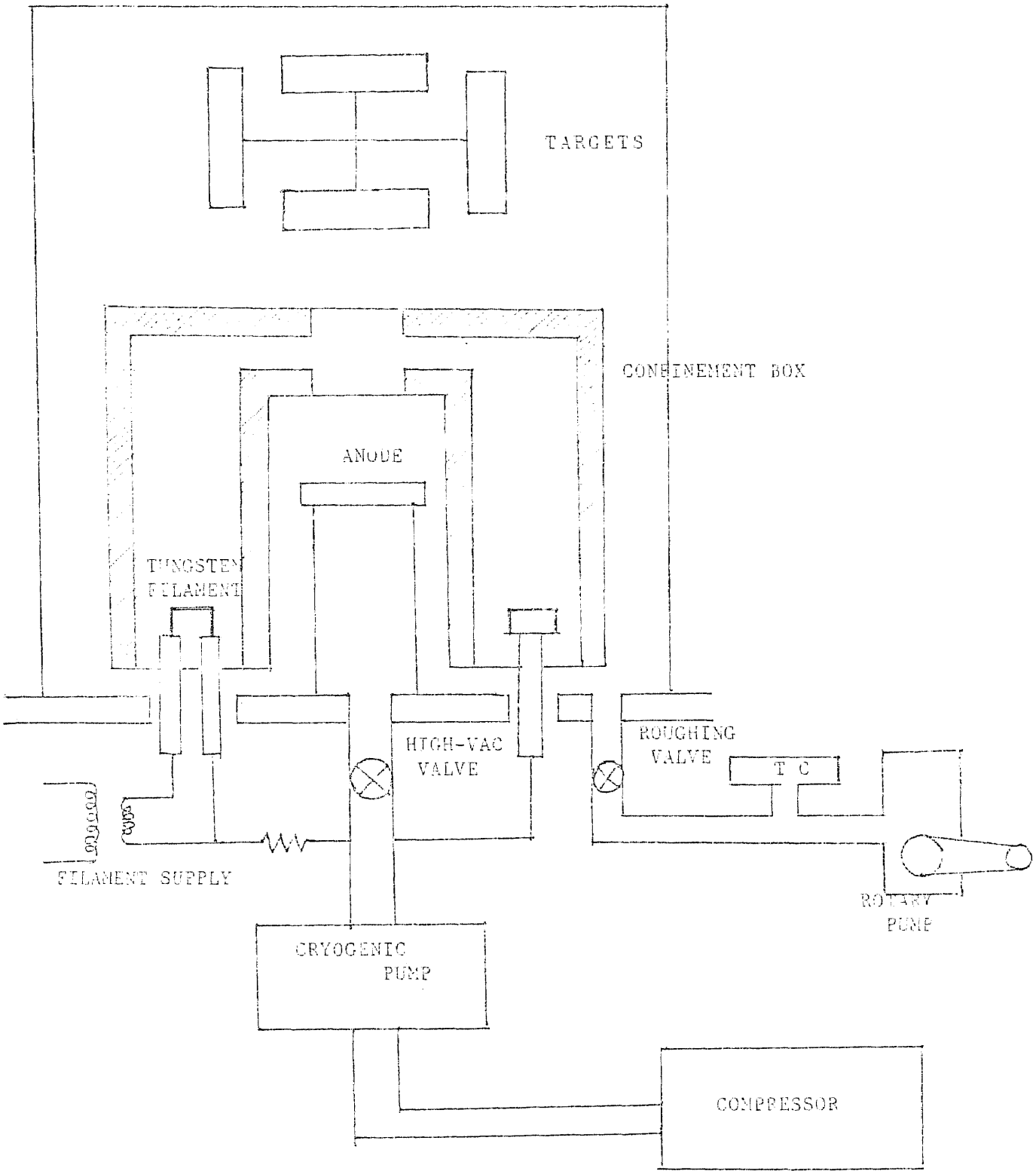

FIG. 5 -2. A SCHEMATIC DIAGRAM OF NRC TRIODE SPUTTERING SYSTEM.

APPENDIX A

Infrared Spectra Using Perkin-Elmer 457 Spectrophotometer

A.1 The nature of the infrared absorption spectrum

i) Conventional spectroscopic techniques are used to observe three main types of molecular transitions, electronic, vibrational and rotational. Electronic transitions are observed in the ultra-violet and visible regions of the spectrum, vibration-rotation transitions in the infrared and pure rotational transitions in the far-infrared and microwave regions. These boundaries are only loosely defined and some overlap occurs.

ii) The characteristic frequencies for a particular molecule are determined by the masses of the constituent atoms, their spatial geometry, and the strengths of the connecting bonds.

iii) The degree of absorption in a function of the change in dipole moment that occurs during a vibration. If no change occurs in the dipole moment, there is no interaction with electromagnetic radiation, and the vibrational mode is not excited. Such a vibrational mode is infrared inactive.

A.2 The procedure for infrared spectrum measurement.

The procedure for optical absorption measurement starts before deposition of the films. This first step, before deposition, evolves the cleaving of a substrate into at least 3 pieces of equal thickness, each of which is larger than the aperture in the spectrometer metal mask. The largest aperture used is 0.75 cm in diameter. Two of these matched substrates are kept for optical references and the remaining portions are used for the deposition.

Once deposition is completed, the two optical references are used to establish a 100% transmission reference. This is accomplished by placing one optical reference in the reference beam of the spectrophotometer and the other in the sample beam. The sample and reference beams are simply the result after mechanically splitting the radiation from a single infrared source. Once the beam is split the operator simply allows the incident infrared radiation to vary from 2.5 to 50 microns in wavelength. The variation in transmission over this range is continuously monitored with the use of the attached strip chart recoder. If the instrument is operated properly, the deviation from the 100% transmission line is not more than 10%. If greater variations occur, the samples are checked for complete coverage of metal mask by the sample.

Once the 100% transmission line is determined, the

optical reference in the sample beam is replaced by the remaining matched substrate previously deposited on. Monitoring of this new pair of samples over the same range of incident energies should yield a scan, from the strip chart recoder, of the optical behavior for the thin film in question.

To assure proper response of the spectrophotometer to sharp increase in absorption coefficient, the slow speed, denoted slow mode, and normal slit, should be used. This will allow as much radiation as possible to vary as slowly as possible thus allowing the equipment to respond properly. Surface defects will allow additional transmission which may not be characteristic of th actual film and make measurement at that particular location on the film impossible.

A.3 The specification of Perkin-Elmer model 457 Spectrophotometer

Prinple	Double beam, optical null, linear transmittance versus linear wavenum ber recording.
Optics	f/5 monochromator, two gratings, reflecting optical system employing planar and aspheric mirrors
Abscissa Range	4000 to 250 cm^{-1}
Ordinate Range	0 to 100% linear in transmission

APPENDIX B

RF Biased RF Sputtering.

Rf biased rf sputtering is carried out with one generator delivering a fixed percentage of its output to collector[1]. The target impedance matching network and driver turning are used to adjust the target sputtering conditions while the anode matching network is actually used to detune the anode in order to obtain proper bias voltage.

An electrical model of the system used for experiments is shown Fig.B-1(2). The three capacitors C_T, C_W and C_S, with associated loss resistances, are the approximate representations of the plasma boundaries at the target, wall and substrate holder respectively(3). The diodes represent the rectifying action which occurs at the plasma boundary due to the higher mobility of ions. As the inductance is varied from zero, the rf impedance between substrate holder and ground decreases to a minimum at series resonance between L and C, and then rises to a maxomum when parallel resonance is reached. Therefore, the impedance between substrate holder and ground can be varied over a wide range. Losses in the substrate impedance will naturally limit the maximum and minimum values of impedance that can be obtained.

A detailed analysis of the circuit of Fig. B-1 is rather difficult because the boundary or sheath impedances

are not constant, but vary with the rf current flow through them. However, a qualitative description of the rf current variation is necessary to understand the experimetal data.

Consider the case for which L is adjusted to be resonant with C (minimum rf impedance). This is approximately the case for a conventional untuned system, except for the presence of a dc blocking capacitor. In this case most of the rf current will flow to the wall, which normally has the largest area, and hence, the lowest impedance. If the inductance L is increased, its reactance will partially cancel the capacitive reactance C_S of the substrate sheath, resulting in a lower net impedance between plasma and ground through thesubstrate holder. The rf current I_S will increase while rf current I_W will decrease. The target rf current I_T is nearly constant, since the impedance between target and plasma is normally quite large. As I_S increases, the rf potential across the substrate sheath increases, as does the rf voltage between substrate holder and ground. A maximum should occur in I_S when the whole path between plasma and ground through the substrate holder reaches a minimum net impedance. This condition will yield the maximum rf and dc potential between substrate and plasma.

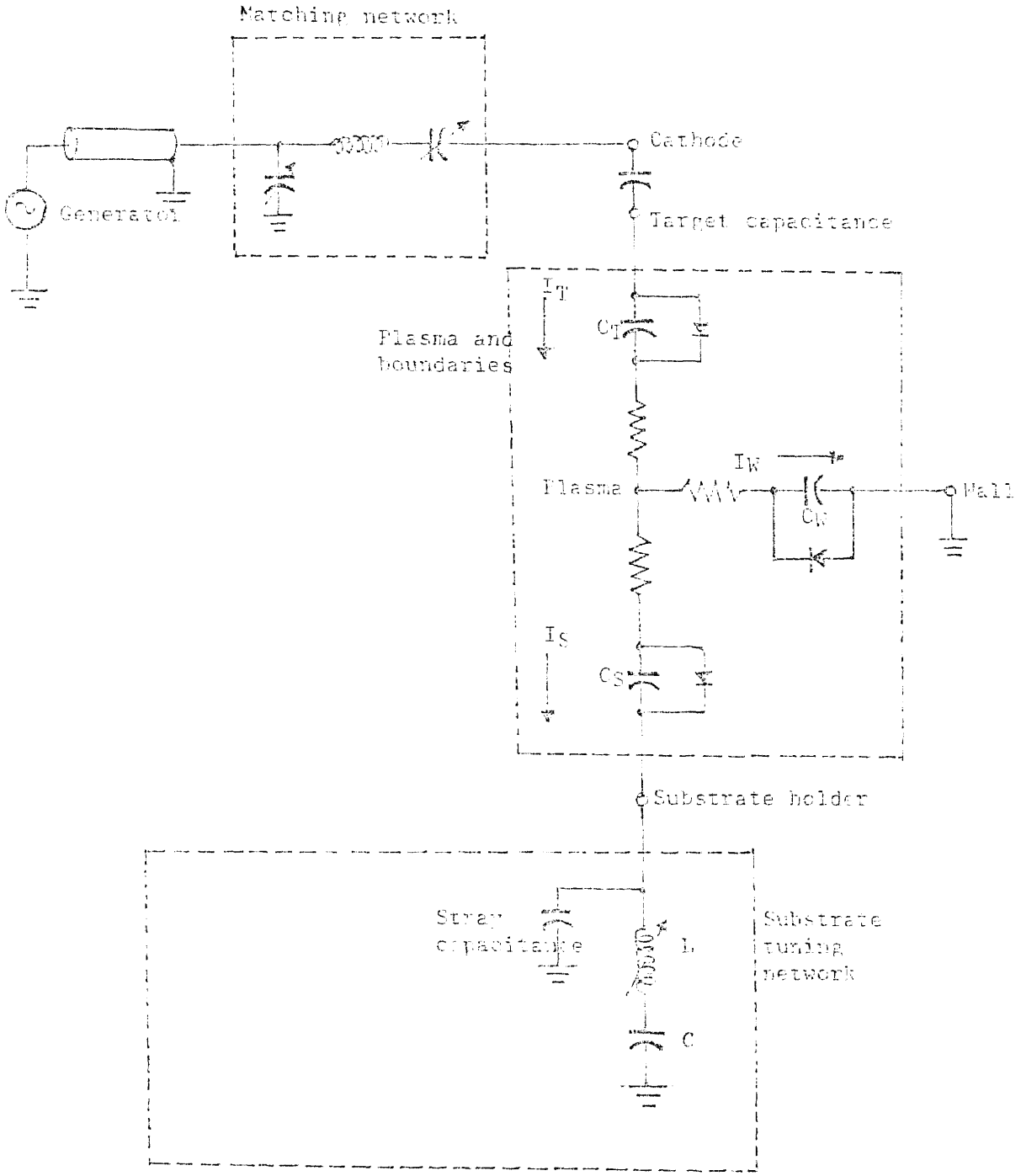

Fig. B-1 Electical model for bias sputtering system

APPENDIX C

Computer program to calculate optical constants n,k from transmittance.

This program has four major functions which are

1. fref(i): calculate refractive index at k=0 at left end and at right end wavenumber.
2. fr(i) : designates the fraction of a light beam travelling interface with the deposted film.
3. FF(nn,kk,i) : calculate the value of derivarative of transmittance and phase shift.
4. est(yy1,yy2,j) : solve two nonlinear equation by Newton method to determine the optical constants from transmittance and phase shift.

```
/* Ip[i] : transmittance of substrate
   I[i]  : transmittance of film      */
/*  Main program */
#include  <stdio.h>
#include  <math.h>
#define   Len 44                    /* number of data set */
#define   ERR 1.0e-4                /* tolerance of error */
#define   Vmin 350                  /* left end wavenumber */
#define   Vmax 1430                 /* right end wavenumber */
float     sq(), fthe(), fr(),FF();  /* functions */
```

```
float     I[Len+1],Ip[Len+1],Dat[Len+1],Ti2[Len+1];
float     n[Len+1],k[Len+1],Va[Len+1],Da[Len+1];
float     ph,d,Rw,h;
/* ph: refractive index of substrate
   d : thickness of film                    */
main(ac,av)
int  ac;
char *av[];
{
        FILE  *fp;
        float temp;
        int   i,j,m;
        d = 1.7e-5;
        Va[0] = Vmin;
        Va[Len] = Vmax;
        ph = 3.4;  /* silicon substrate index of refraction*/
        Rw = sq((ph-1)/(ph+1));
/* Read data and calculate transmittance Ti2[i] */
        if ((fp = fopen("data","r") <= NULL) {
             printf ("\n cannot open data file \n);
             exit();
        }
        for (i = 0; i <= Len; i++) {
             fscanf (fp,"%f %f", &I[i],&Ip[i]);
             Ti2[i] = sqrt((I[i] / Ip[i] / ph) * (1. - Rw));
             Dat[i] = log(Ti2[i]);
        }
```

```
        fclose(fp);
/* Calculate n_L at left end and n_R at right end wavenuber*/
        m = 0;
        fref (m);
        m = Len;
        fref (m);
/* Calculate phase shift by Simpson's rule */
        h = (Vmax - Vmin) / Len;
        Va[Len - 1] = Vmin + (Len - 1) * h;
        Da[Len - 1] = fthe(Va[Len - 1],Len-1);
/* Calculate theta at each frequency by T */
        for (j=1;j<Len;j++) {
             n[j]=[j-1];k[j]=k[j-1];
             Va[j] = Vmin + j * h;
             Da[j] = fthe(Va[j],j);
/* Incccrease theta to true value which is based on previous
result */
             temp = (Va[j] - Vmin) / (Vmax - Vmin);
             Da[j] += ((1.0 - temp) * (Da[0] - Da[1]));
             Da[j] += (temp * (Da[Len] - Da[Len - 1]));
/* Calculate n,k at each frequency */
             est (&n[j],&k[j],j);
        }
for (j = 0; j <= Len; j++) {
printf ("\n %f %f %f %f %f %f",Va[j],I[j],Ip[j],n[j],k[j]);
}
}
```

```
/* function est(yy1,yy2,j) solves two nonlinear equations*/
   est(yy1,yy2,j)
{
        for(ii = 1; ii < IMAX; ii++) {
        FF(x,y,j,&f0,&f1,&f2,&g0,&g1,&g2);
        ss = f1 * g2 - f2 * g1;
        dx = (f0 * g2 - g0 * f2)/ss;
        dy = (g0 * f1 - f0 * g1)/ss;
        x1 = x - (f0 * g2 - g0 * f2)/ss;
        y1 = y - (g0 * f1 - f0 * g1)/ss;
        if (fabs(x1-x) <= ERR && fabs(y1-y) < ERR) break;
        else { x = x1; y = y1}
        }
*yy1 = x1;
*yy2 = y1;
return;
}
/* function fthe(tem,i) calculates the phase shift by
Simpson's rule */
float  fthe(tem,i)
float  tem;
int    i;
{
        sum = 0.0;
        vt = Vmin;
        for ( i = 1; i < Len; i++) {
```

```
            vt = vt + h;
            if(fabs(vt-tem) < h/100)  { vt += h; i++;}
            if (( (int) (i/2) * 2) == i)
                  sum += 4.0 * Dat[i] / (sq(vt) - sq(tem));
            else
                  sum += 2.0 * Dat[i] / (sq(vt) - sq(tem));
      }
ba = Dat[0] / (sq(Vmin) - sq(tem));
bo = Dat[Len] / (sq(Vmax) - sq(tem));
area = -Dat[0] / M_PI * log(nn * h / (2.0 * Vmin + nn * h));
area -= Dat[Len] / M_PI * log ((2.0 * Vmin + (Len + nn * h)
/ ((Len - nn) * h));
area -= 2.0 * tem / M_PI * ( ba + sum +bo) * h / 3.0;
area += 2.0 * M_PI * tem * d;
return (area);
}

/* funtion fref(i) calculates refractive index at k=0 */
fref(i)
int i;
{
      temp = Ti2[i];
      for (m=2;fabs(in[m-1] - in[m-2]) > 0.05; m++) {
      n[i] = m * 0.1 + 2.0;
  do  {
      T2 = temp;
```

```
        for ( ii = 0; ii < 100; ii++) {
        FF1 (n[i],k[i],i,&f0,&f1);
        if (fabs(f0) < ERR) break;
        n[i] -= f0/f1;
        }
    Da[i] = atan((k[i] * C + n[i] * D)/(n[i] * C - k[i] * D));
    temp = sqrt((I[i]/Ip[i]/ph) * ((1. - fr(n[i],k[i],i) * Rw)
    / (1. + Rw));
    } while ( fabs(T2 - temp) > ERR);
    T2 = temp;
    in[m] = n[i];
}
```

BIBLIOGRAPHY

1.1 R.J.Temkin, W.Paul, and G.A.N.Connell, Adv. Phys. 22,581(1973)

1.2 M.H.Brodsky, R.S.Title, K.Weiser, and G.D.Pettit, Phys. Rev. B1, 2632(1970)

1.3 W.Paul, G.A.N.Connell, and R.J.Temkin, Adv. Phys. 22, 529(1973)

1.4 A.J.Lewis, Phys. Rev. B14,658(1976)

1.5 G.A.N.Connell, and J.R.Pawlik, Phys.Rev. B13,787(1976)

1.6 T.D.Moustakas and William Paul, Phys. Rev. B16, 1564(1977)

2.1. L.Banyaz, Proc. Intern. Conf. Semiconductor Physics, Paris,1964,Academic Press, New York, p417

2.2. N.F.Mott, Advan. Phys., 16, 49(1967)

2.3. A.K.Jonscher, Thin Solid Films, 1,213(1967)

2.4. P.A. Walley and A.K.Jonscher, Thin Solid Films, 1,367(1967)

2.5. J. Frenkel, Phys.Rev., 54,647 (1938)

BIBLIOGRAPHY

2.6. C.A.Mead, Phys.Rev.,128,2088(1962)

2.7. H.Hirose and Y.Wada, Japan J.Appl.Phys.,4,639(1965)

2.8. N.F.Mott and R.W.Gurney, Electronic Processes in Ionic Crystals,Oxford Univ. Press, Oxford,1948

2.9. M.A.Lampert, A.Many and E.Mark, Phys.Rev, 135,A1444(1964)

3.1. M.H.Brodsky and R.S.Title, Phys.Rev.Lett. 23,581(1969)

3.2. S.J.Hudgens, Phys.Rev. B 14,1547(1976)

3.3. G.A.N.Connell and J.R.Pawlik, Phys.Rev. B13,787(1976)

3.4. R.C.Chittick, J.Non-Cryst.Solids 3,255(1970)

3.5. W.Paul,A.J.Lewis,G.A.N.Connell and T.D.Moustakas, Solid State Commun. 20,969(1976)

3.6. M.H.Brodsky and J.J.Cuomo,IBM Tech.Dis.Bul. 19,4802(1977)

3.7. W.E.Spear and P.G.Lecomber, Solid State Commun. 17 , 1193(1975)

3.8. W.E.Spear and P.G.Lecomber,Philos.Mag. 33,935(1976)

BIBLIOGRAPHY

3.9. M.H.Brodsky,Manual Cardona,and J.J.Cuomo,Phys. Rev. B, 16,3556(1972)

3.10. L.J.Bellamy,The Infrared Spectra of Complex Molecules (Chapman and Hall,London,1975) p380

3.11. R.A.Rudder,J.W.Cook,Jr.,and G.Lucovsky,Appl.Phys.Lett. 43,871 (1983)

4.1. I. Simon, J. Opt. Soc. Am. 41,336 (1951)

4.2. T.S.Robinson and W.C.Price "Molecular spectroscopy" edited by G.Shell (The Institute of Petroleum, London) (1955)

4.3. P.N.Schatz, Shiro Maeda and Kunio Kozima, The journal of chemical physics 38, 2658 (1963)

4.4. S.Maeda, G.Thyagarajan, and P.N.Schatz, The journal of chemical physics 39, 3474 (1963)

4.5. O.S.Heavens "Optical Properties of Thin Solid Films" (Academic press Inc., New York, 1955)

4.6. K.Kozima, W.Suetaka, and P.N.Schatz, Journal of the optical society of America 56, 181 (1966)

4.7. Shiro Maeda and P.N.Schatz, Journal of the optical society of America 56,181 (1966)

5.1. R.E. Honing, J.Appl.Phys., 29,549(1958)

5.2. A. Benninghoven, Z. Physik, 220, 159(1969)

BIBLIOGRAPHY

5.3. L.I. Maissel an P.M. Schaible, J.Appl.Phys., 36,237(1965)

5.4. D.M. Mattox, Electrochem. Technol., 2,295(1964)

5.5. J.L. Vossen and J.J. O'Neill,Jr., RCA Rev., 29,566(1968)

5.6. J.S. Logan, IBM J.Res.Develop., 14,172(1970)

5.7. J.L. Vossen, J. of Vac. Sci. and Technol.,8,s12(1971)

B.1. R.B.McDowell "Design consideration for Radio Frequency Sputtering Equipment and Impedance Matching network", Solid State Tech., 12(1969)

B.2. J.S.Logan, Solid State Tech., Dec.1970 p46

B.3. H.R.Koenig and L.I.Maissel, IBM J.Res.Develop.

14,168(1970)